Title:

Strand swapping in the LolA-like protein GerS promotes the allosteric activation of a bacterial amidase in *Clostridioides difficile*

Authors:

Jacob M. Bouchier[1] and Aimee Shen[1]

Affiliations:

[1]Department of Molecular Biology and Microbiology, Tufts University School of Medicine, Boston, MA, USA

Running head: Strand-swapping in GerS promotes the allosteric activation of CwlD

[#]Corresponding author:

aimee.shen@tufts.edu

(617)636-3792

Abstract:

GerS is a key lipoprotein regulator of *Clostridioides difficile* spore germination that shares structural, but not sequence, similarity to LolA in Gram-negative bacteria. GerS and LolA have vastly different biological roles: LolA functions in the trafficking of lipoproteins across the periplasmic space to the outer membrane of Gram-negative bacteria, while GerS allosterically activates the germination-specific amidase CwlD in endospore-forming Gram-positive bacteria. Here, we explore the diversity of LolA-like proteins across bacteria and reveal that GerS homodimer formation is a conserved feature of Peptostreptococcaceae family orthologs. Since dimerization of *C. difficile* GerS occurs via strand-swapping, we sought to investigate the functional importance of its strand swap by identifying mutations that alter the GerS dimer:monomer equilibrium. Our analyses reveal that $GerS^{K71R}$ and $GerS^{N74L}$ substitutions in the strand-swap hinge of GerS stabilize the homodimer, while a $GerS^{T72P}$ substitution promotes monomer formation. Conversely, substituting the highly conserved proline at the equivalent site in LolA for threonine converts LolA from a monomer to a homodimer. Since our data indicate that destabilizing the GerS dimer impairs both GerS:CwlD binding *in vitro* and CwlD function in *C. difficile*, strand-swapped dimer formation in LolA-like proteins enhances their affinity for their binding partners. These data are consistent with analyses of equivalent LolA mutants in *E. coli* and thus provide new insight into the evolution and specialization of this intriguing group of proteins across the bacterial domain.

Introduction

The InterPro homologous superfamily "Prokaryotic lipoproteins and lipoprotein localization factors" (PLLLF; SSF89392) encompasses a group of structurally similar proteins that are widely distributed across the bacterial domain. While some proteins of this group function as anti-sigma factors [1,2], most function as chaperones for transporting proteins or glycolipids across the periplasmic space of diderm bacteria. For example, LolA, the archetypal PLLLF protein, functions within the Lol system (LolABCDE) to facilitate lipoprotein trafficking across the periplasm in diderm bacteria [3–9], while LppX [10], LprG [11], and LprF [12] transport various glycolipids across the periplasm of *Mycobacterium* spp. In contrast, PLLLF proteins in endospore-forming monoderm bacteria seem to have evolved specialized roles in sporulation and germination. For example, SsdC from *Bacillus subtilis* forms a ring-like structure in the forespore that functions in the development of spore shape [13], and GerS regulates spore germination in *Clostridioides difficile* [14].

Spore germination depends on the enzymatic degradation of the cortex, a protective layer of modified peptidoglycan that maintains metabolic dormancy [15,16]. The cortex lytic enzymes that degrade the cortex recognize spore-specific peptidoglycan modifications found exclusively within the cortex, namely muramyl-δ-lactam (MAL) [17]. The specificity of these enzymes for MAL limits their degradative activities to the cortex layer. MAL is made by the coordinated activities of the germination-specific amidase CwlD and the peptidoglycan deacetylase PdaA [18–21]. While *B. subtilis* CwlD has intrinsic activity, *C. difficile* CwlD requires an additional factor to license its activity, the GerS lipoprotein [22,23]. GerS forms a 1:1 complex with CwlD and allosterically activates CwlD's amidase activity by stabilizing CwlD's binding to its Zn^{2+} cofactor [23]. This interaction is essential for germination because deletion of *gerS* abolishes spore germination in *C. difficile* [14] and disruption of a salt bridge formed between aspartate 106 of GerS and arginine 169 of CwlD reduces germination [23]. However, the reduction in *C. difficile* spore germination caused by the GerS D106R substitution is relatively

subtle, even though it significantly reduces binding to CwlD *in vitro* [23]. These data indicate that additional factors beyond the salt bridge regulate the GerS:CwlD interaction and thus the amidase activity of CwlD.

In the crystal structure of the GerS:CwlD complex, GerS forms a homodimer via a strand-swap mechanism [23]. Strand swapping, a specific form of domain swapping [24–31], is a dimerization mechanism in which one or more β-strands are exchanged between two proteins [32]. Dimerization via strand swapping is observed in the dimeric structures found in the light chain subunits of immunoglobulins [33] and cystatins [34], and it is thought to be associated with pathogenic amyloid fibril formation in humans [35–37]. Strand swapping can also regulate protein function [38]. For example, monomeric human cystatin C inhibits cathepsin B, but its strand-swapped dimer loses this ability [39], and strand swapping in cadherins facilitates cell-cell adhesion, forming weak, reversible interactions [28,40]. However, the functional significance of strand swapping in GerS on the allosteric activation of CwlD by GerS remains unclear.

Notably, *C. difficile* GerS is the only known PLLLF protein that naturally dimerizes via a strand swap mechanism, whereas LolA from *Escherichia coli* can be induced to dimerize when Phe68 is substituted with Glu, which induces a similar strand swap [41,42]; the F68E substitution was designated F47E based on the sequence after lipoprotein signal peptide processing. This mutation is toxic to *E. coli* because $LolA^{F68E}$ binds LolC too tightly and prevents proper lipoprotein trafficking to the outer membrane [42]. Here, we test the impact of strand swapping in GerS on CwlD function. By identifying mutations that shift the GerS dimer:monomer equilibrium, we demonstrate that strand-swapping in GerS stabilizes its interaction with CwlD and promotes the allosteric activation of this important amidase. Our analyses provide molecular insight into the mechanisms that allow for strand swapping and highlight the general role of these structures in regulating adhesive interactions.

Results

93

94 **PLLLF proteins maintain low sequence identity but high sequence similarity and**
95 **structural similarity.**

96 With the goal of identifying the underlying and shared features between GerS and the
97 rest of the PLLLF superfamily, we analyzed the evolutionary relatedness of proteins within the
98 group. We found that heuristic search methods, such as BLASTp, were inadequate for
99 identifying members of this group. Instead, we employed probabilistic searches using InterPro
100 and structural searches using FoldSeek to identify which major bacterial classes contain
101 bacteria that encode PLLLF proteins [43–46]. We then generated a phylogenetic tree using core
102 genes across species based on the major bacterial classes that have species encoding PLLLF
103 proteins (Supplemental Figure 1). Remarkably, we found that PLLLF proteins are widespread
104 across the bacterial domain. Further, we found that the presence of PLLLF proteins is
105 independent of whether the bacteria are monoderms or diderms (Supplemental Figure 1),
106 suggesting that not all PLLLF proteins function in a similar way to LolA.

107 Using AlphaFold 3 [47], we predicted the structure of 17 representative PLLLF proteins
108 and aligned them using DALI [48]. Using this structural alignment, we compared sequence
109 identity and sequence similarity across the proteins. Despite sharing little sequence identity, the
110 sequence similarity across PLLLF group members is high (Figure 1A). Together, these
111 observations indicate that PLLLF proteins are highly conserved and suggest that they share
112 evolutionary ancestry, although they likely evolved specialized roles within diderms vs.
113 monoderms.

114

115 **GerS strand swapping is unique among characterized PLLLF proteins.**

116 While AlphaFold 3 [47] predicts that GerS adopts a structure remarkably similar to other
117 PLLLF proteins, the GerS-CwlD crystal structure shows that GerS forms a homodimer via a
118 strand-swap mechanism (Figure 1B)[23]. Crystal structures of other PLLLF proteins, ranging

119 across several bacterial classes, suggest that PLLLF proteins exist either as monomers or
120 heterodimers with other proteins but rarely as homodimers [3,5,10,11,49,50].
121 While LolA does not form homodimers naturally, a single substitution of phenylalanine to
122 glutamate at residue 68 (F68E, previously published as F47E based on numbering from the
123 lipobox) is sufficient to induce homodimerization [42]. This homodimerization is achieved by
124 converting a β-turn into a strand-swap hinge, which is remarkably similar to the strand swap
125 observed in GerS (Figure 1C, Supplemental Figure 2). Notably, the $LolA^{F68E}$ variant binds its
126 interacting partner LolC with increased affinity, but this enhanced affinity interferes with LolA's
127 ability to bind the lipoprotein substrates that it normally transports across the periplasm,
128 rendering the $LolA^{F68E}$ variant toxic to *E. coli* [41,42]. Based on these observations, we
129 hypothesized that strand swap-mediated dimerization of GerS stabilizes GerS binding to CwlD
130 and promotes CwlD binding to its Zn^{2+} co-factor.
131
132 **Dimerization is conserved in GerS orthologs of the Peptostreptococcaceae family.**
133 Since CwlD is widely conserved in endospore-forming bacteria, we first assessed the
134 conservation of *gerS* among the Firmicutes, the only known class to contain endospore-forming
135 bacteria like *C. difficile* and *Bacillus subtilis*. To avoid issues associated with identifying PLLLF
136 proteins through heuristic methods like BLASTp, we instead used synteny-based searches such
137 as GeCoViz [51] and BioCyc genome alignment [52] to find GerS orthologs; we confirmed their
138 structural homology using AlphaFold3-predicted structures and ChimeraX (Figure 2A;
139 Supplemental Figure 3) [47,53].
140 Six orthologs were selected for further characterization from Firmicutes species that
141 sporulate and encode a GerS ortholog. To investigate dimerization, each ortholog was
142 expressed in *E. coli* and purified for analysis via size-exclusion chromatography (SEC). The
143 SEC trace of GerS from *Clostridioides difficile* revealed two distinct peaks, which represent the
144 monomeric and homodimeric forms of the protein ([23], Figure 2B; Supplemental Figure 4).

145 Notably, two other Firmicutes, *Paraclostridium bifermentans* and *Paraclostridium sordellii*
146 (formerly *Paeniclostridium sordellii* [54]), exhibited similar SEC profiles, indicating that they also
147 form homodimers. In contrast, GerS orthologs from *Clostridium aceticum*, *Gottschalkia acidurici*,
148 and *Clostridium perfringens* displayed a single peak corresponding to the monomeric form.
149 Since *P. bifermentans* and *P. sordellii* are members of the Peptostreptococcaceae family like *C.*
150 *difficile*, unlike the other species tested, these data suggest that GerS dimerization is specific to
151 the Peptostreptococcaceae family.
152 We also identified GerS orthologs in the Bacilli class, but they are distinguished by an
153 additional domain of unknown function (DUF4367). We purified the *Bacillus subtilis* ortholog,
154 previously published as SsdC [13], with and without the DUF4367 domain and analyzed the two
155 variants via SEC. Although both traces had two peaks, Coomassie staining of earlier eluting
156 fractions revealed proteins larger than the expected size for SsdC that are likely chaperones
157 (Supplemental Figure 4B-C), indicating that SsdC primarily exists as a monomer *in vitro* and
158 that the DUF4367 domain does not prevent SsdC dimerization. Thus, GerS dimerization is
159 limited to the Peptostreptococcaceae family.
160
161 **Mutations in the strand-swap hinge alter GerS dimer stability.**
162 To determine the role of the strand swap in regulating GerS dimerization and function,
163 we aimed to identify mutations that destabilize the GerS dimer. Previous studies have shown
164 that mutations that disrupt the 'hinge' region of the swapped strand can prevent dimerization
165 (Figure 3A) [28,29,55–57]. While these studies have also shown that it can be difficult to predict
166 which residue will alter a given dimer:monomer equilibrium, we reasoned that replacing the
167 hinge of GerS with the equivalent sequence found in a monomeric PLLLF protein like LolA
168 might prevent GerS dimerization. To this end, we used AlphaFold3 to predict the monomeric
169 structure of GerS and aligned it with the LolA crystal structure (PDB 1IWL). This alignment
170 revealed that the GerS strand-swap hinge, Lys71-Thr72-Asp73-Asn74 (KTDN), lies in a similar

171 position to LolA Arg64-Pro65-Asn66-Leu67 (RPNL; Figure 3B). We then tested the effect of
172 replacing individual amino acids in the *C. difficile* GerS hinge with the analogous residues in the
173 *E. coli* LolA region. Intriguingly, replacing Thr72 with Pro increased the proportion of GerS in the
174 monomeric form, while replacing Lys71 with Arg and Asn74 with Leu increased the dimeric form
175 (Figure 3C; Supplemental Figure 5A). In contrast, the GerS^{D73N} variant precipitated quickly after
176 purification and co-purified with the chaperones from *E. coli* (Supplemental Figure 5B)[58–60],
177 strongly suggesting that the substitution destabilized GerS.

178 Since the GerS^{K71R} and GerS^{N74L} variants favored the dimeric form relative to WT GerS
179 (Figure 3C-D), we purified the dimeric fractions and re-analyzed them by SEC to compare the
180 relative stabilities of the GerS homodimers formed by each variant. The re-purified GerS^{K71R} or
181 GerS^{N74L} variants again showed a higher dimer-to-monomer ratio than WT GerS (Supplemental
182 Figure 6A-B), indicating that the K71R and N74L substitutions enhance the stability of the GerS
183 homodimer structure.

184

185 **Proline substitutions in the strand-swap hinge destabilize the GerS homodimer.**

186 Since GerS^{T72P} favors the monomeric form compared to WT GerS (Figure 3C-D), we
187 next tested the effect of changing the other hinge residues to proline. Previous studies have
188 found that introducing prolines into the strand-swap hinge affects dimerization in a wide range of
189 proteins across all domains of life [28,29]. For example, highly conserved prolines in the loops
190 of *Mycobacterium tuberculosis* BlaC maintain BlaC in a monomeric and functional form,
191 whereas substitutions of these residues result in dimerization and loss of function [61]. When
192 the other hinge residues of GerS were replaced with proline (K71P, D73P, and N74P), all three
193 substitutions appeared to destabilize GerS (Figure 4A), and the resulting variants were quick to
194 crash out of solution. The D73P and N74P substitutions resulted in low protein yields, while
195 SEC analyses of the GerS^{K71P} variant revealed that it copurified with *E. coli* proteins likely to be

196 chaperones (Supplemental Figure 7B). Thus, the location of the proline substitution is critical for
197 regulating the GerS dimer-to-monomer equilibrium.

198 Consistent with this finding, analysis of the conservation of hinge prolines among PLLLF
199 proteins using the DALI alignment revealed that three proline residues are highly conserved
200 among this superfamily, and each of these prolines correspond to beta-turns in PLLLF proteins
201 (Figure 4B). Notably, GerS contains two of these conserved prolines but not the conserved
202 proline at residue 72 (Figure 4C). Together, these observations highlight how a proline at this
203 location destabilizes the GerS homodimer and promotes GerS monomer formation.

204 To test whether the conserved proline in the analogous position of other monomeric
205 PLLLF proteins regulates dimerization, we substituted the *E. coli* LolA Pro65 with a Thr (P65T).
206 Remarkably, while wild-type LolA eluted as a monomer, $LolA^{P65T}$ eluted primarily as a dimer
207 (Figure 4D). Taken together, these data highlight how a proline at this site promotes β-turn
208 formation and thus the monomeric form, consistent with past studies of β-turns [62,63].

209 While the T72P substitution effectively shifted the dimer-to-monomer equilibrium toward
210 the monomer state, it did not completely prevent the formation of GerS homodimers (Fig 3C,
211 4A). To further destabilize the dimer, we introduced a second proline at the fourth residue,
212 creating the hinge sequence Lys71-Pro72-Asp73-Pro74 (KPDP). Since prolines in β-turns are
213 often paired with flexible glycine residues to counteract their rigidity [63–65], we also replaced
214 the first and third residues in the hinge with glycines, yielding a Gly71-Pro72-Gly73-Pro74
215 (GPGP) hinge sequence. The $GerS^{KPDP}$ variant eluted as a single peak at a volume that falls
216 between the dimer and monomer peaks, suggesting that the variant interconverts between the
217 monomer and dimer forms as it is resolved on the column, whereas the $GerS^{GPGP}$ variant
218 exclusively eluted as a monomer (Figure 4E). These results indicate that the addition of a
219 second proline in the strand-swap hinge further destabilizes the GerS homodimer—favoring the
220 monomeric form—especially when glycines are introduced to provide greater conformation
221 flexibility.

222 **Decreasing GerS dimer formation reduces its affinity for CwlD and impairs *C. difficile***
223 **spore germination**

224 Since we originally hypothesized that strand-swapping in GerS enhances its ability to
225 bind CwlD based on analyses of other strand-swapped proteins [42], we next tested if
226 destabilizing the homodimer affects its affinity for CwlD. To this end, we co-affinity purified His_6-
227 tagged CwlD with untagged GerS variants and analyzed their interactions by SEC. Untagged
228 $GerS^{WT}$, $GerS^{K71R}$, and $GerS^{N74L}$ co-purified efficiently with His_6-tagged CwlD and eluted as the
229 GerS:CwlD complex as well as the GerS and CwlD monomers in SEC analyses (Figures 5A,B,
230 Supplementary Figure 8). It should be noted that the GerS:CwlD complex eluted as several
231 peaks due to the higher resolution SEC performed relative to our prior work [23].

232 Since the K71R and N74L substitutions stabilized GerS homodimerization, we
233 considered the possibility that these variants may bind CwlD more tightly than wild-type GerS.
234 To test this, we resolved co-purifications of $GerS^{K71R}$:CwlD-His_6 and $GerS^{N74L}$:CwlD-His_6 using
235 SEC, collected the dimer fractions, and re-resolved them through SEC again (Supplemental
236 Figure 9). To our surprise, the $GerS^{K71R}$ and $GerS^{N74L}$ variants formed weaker interactions with
237 CwlD-His_6 than wild-type GerS. However, the differences between $GerS^{K71R}$ and $GerS^{WT}$ were
238 subtle. We next attempted to further stabilize the GerS dimer by replacing the GerS hinge with
239 the hinge (QVVAG) from the strand-swapping cystatin, Stefin B, because this hinge was
240 previously reported to reliably form domain-swapped homodimers [66]. However, substituting
241 GerS's hinge region for Stefin B's hinge region ($GerS^{QVVAG}$) destabilized GerS, causing it to
242 quickly crash out of solution; indeed, the SEC trace matched that of the unstable D73N
243 substitution (Supplemental Figure 10), and untagged $GerS^{QVVAG}$ failed to copurify with CwlD-
244 His_6 (Supplemental Figure 10B). Therefore, the effect of stabilizing the GerS homodimer on
245 CwlD remains unclear.

246 In contrast to $GerS^{K71R}$ and $GerS^{N74L}$, considerably less $GerS^{T72P}$ co-purified with His_6-
247 tagged CwlD (Figure 5A, Supplementary Figure 7). In addition, when the co-purification was

248 resolved by SEC, no GerS^{T72P}:CwlD-His$_6$ complex was observed, indicating that the co-affinity
249 purified complex was not stable during SEC (Supplementary Figure 8). These latter data
250 indicate that destabilizing the GerS homodimer decreases its binding to CwlD. Consistent with
251 this conclusion, the GerS^{KPDP} and GerS^{GPGP} variants, which favor the monomeric form (Figure
252 4E), had even lower affinity for CwlD-His$_6$ (Figure 5B).

253 To determine the impact of preventing GerS dimerization on GerS function during *C.*
254 *difficile* germination, we complemented our Δ*gerS* mutant with constructs encoding dimer-
255 breaking GerS mutations and measured their effects on GerS stability and spore germination
256 efficiency. While GerS^{K71R} and GerS^{N74L} interacted with CwlD at the same levels as wild-type
257 GerS *in vitro*, both variants were detected at lower levels in sporulating cells compared to the
258 Δ*gerS* wild-type complement. Additionally, both mutants were almost undetectable in purified
259 spores (Figure 5C). Consistent with our previous findings that interaction with CwlD stabilizes
260 GerS [23], very low levels of the GerS^{GPGP} variant were detected in sporulating cells, and we
261 were unable to detect this variant in purified spores (Figure 5C). However, the GerS^{T72P} variant
262 and GerS^{KPDP} variant were readily detectable in both sporulating cells and purified spores,
263 implying that their ability to interact with CwlD is sufficient to stabilize the GerS variants in
264 spores (Figure 5C).

265 Notably, even though the dimer-disrupting strand-swap mutations decreased GerS
266 levels in mature spores, the GerS dimerization mutants exhibited only an ~2-fold decrease in
267 germination ($p < 0.00005$, Figure 5D). This finding is consistent with our prior work indicating
268 that a GerS mutation, D106R, which disrupts a salt-bridge at the interaction interface of GerS
269 and CwlD, results in a modest but significant decrease in germination [23]. Our results also
270 suggest that relatively GerS is needed in spores to license CwlD amidase activity.

271

272 **Interaction with CwlD requires both strand swapping and a salt bridge.**

273 Since our analyses revealed that GerS mutants defective in dimerization still allow for *C.*
274 *difficile* germination to proceed, additional features of GerS beyond strand-swapping allow GerS
275 to bind CwlD. Indeed, our *in vitro* analyses revealed that GerS dimerization mutants can still co-
276 purify with CwlD-His_6, albeit at greatly reduced levels (Figure 5B). Since we previously showed
277 that the interaction between GerS and CwlD is partially dependent on a salt bridge that forms
278 between arginine 169 of CwlD and aspartate 106 of GerS [23], we reasoned that GerS binding
279 to CwlD may depend on both the salt bridge and GerS strand swap (Figure 6A). To test this
280 possibility, we combined the salt-bridge and strand-swapping mutations to generate
281 $GerS^{T72P,D106R}$, $GerS^{KPDP,D106R}$, and $GerS^{GPGP,D106R}$ variants. Remarkably, these combined
282 mutations fully disrupted GerS binding to CwlD, since the untagged GerS variants were not
283 detectable in the co-elutions with His_6-tagged CwlD (Figure 6B). Consistent with this finding,
284 purified spores from Δ*gerS* strains complemented with constructs encoding the combined salt-
285 bridge and strand-swap mutations failed to germinate (Figure 6C), presumably due to their
286 inability to bind CwlD and allosterically activate its amidase activity during cortex modification
287 [23]. In addition, the combined mutations greatly decreased GerS levels even in sporulating
288 cells (Figure 6D). Taken together, our data highlight the importance of both the strand swap and
289 salt bridge on GerS binding to CwlD and, by extension, regulation of *C. difficile* spore
290 germination.
291

292 **Discussion**

293 Our prior discovery that the *C. difficile* GerS lipoprotein binds the CwlD amidase as a
294 strand-swapped dimer led to the question of whether strand-swapping by GerS enhances its
295 ability to allosterically activate the CwlD amidase [23]. By identifying mutations that shift the
296 GerS dimer:monomer equilibrium to the monomeric form (Figure 3), we show that monomeric
297 GerS has greatly reduced affinity for its binding partner, CwlD, which in turn reduces, but does
298 not abolish, *C. difficile* spore germination (Figure 5). Since combining monomer-promoting

299 mutations with a mutation that disrupts a salt-bridge at the GerS:CwlD interface abrogates
300 GerS's ability to activate the CwlD amidase, our data reveal a critical role for GerS's hinge
301 region in regulating the allosteric activation of CwlD.

302 While our findings are consistent with prior work highlighting that strand-swapping can
303 stabilize adhesive interactions, such as in cadherins and the $LolA^{F68E}$ variant, they also raise the
304 possibility that the dynamic instability of the strand-swapped dimer, which exists in near-equal
305 proportions with the monomeric form *in vitro* (Figure 3), contributes to GerS function. Strand
306 swapping is sometimes the result of localized unfolding around the hinge. While the rest of the
307 protein folds, the strand to be swapped unfolds, leading to monomeric and dimeric
308 conformations [32,67]. Like GerS, the yeast cell-cycle regulation protein $p13^{suc1}$ has both a
309 native monomer and dimer state [29]. Two prolines in the hinge generate tension in each state,
310 functioning as a sort of spring between both the monomer and dimer conformation.
311 Substitutions in the hinge of the swapped structure shift the equilibrium of the dimer and
312 monomer populations [29]; in a similar manner, the K71R and N74L substitutions in GerS
313 stabilize the dimeric conformation, while the T72P and GPGP substitutions stabilize the
314 monomeric conformation. The persistence of the two stable populations in near equal
315 proportions suggests that the GerS monomer may be functionally important, perhaps to ensure
316 that GerS transiently interacts with CwlD during MAL formation. Alternatively, additional
317 regulatory factors may influence or stabilize one conformation over the other during this
318 process.

319 Our finding that replacing the GerS strand-swap hinge with the corresponding region
320 from Stefin B [66] destabilizes the protein (Supplemental Figure 10) suggests that dimerization
321 in these proteins depends on distinct, non-interchangeable hinge features. While most domain-
322 swapped proteins have hinge loops of four to five residues, they otherwise vary widely in
323 sequence and structure. Nonetheless, a common feature is that these hinges originate from β-
324 turns in their monomeric structures [38,68,69]. Consistent with previous findings that conserved

325 prolines in β-turns can prevent deleterious strand-swapping in *M. tuberculosis* BlaC [61], we
326 found that the introduction of prolines into the GerS hinge destabilizes the strand-swapped
327 dimer (T72P, GPGP; Figure 4)[61]. Yet, there are also examples where introducing prolines into
328 β-turns instead promotes domain swapping [70–72]. Together, these findings underscore that
329 there is no universal "syntax" for strand swapping and that structural states must be empirically
330 determined on a case-by-case basis.

331 The fact that a single threonine-to-proline substitution in the GerS hinge dramatically
332 alters its conformational stability implies that PLLLF proteins may have evolved inherent
333 instability at this site, potentially enabling their structural flexibility. Although *C. difficile* and *E.*
334 *coli* diverged billions of years ago [73], a reciprocal substitution at the same hinge position in
335 LolA ($LolA^{P65T}$) is sufficient to shift the protein from a monomer to a strand-swapped dimer
336 (Figure 4). This evidence, along with the similarly strand-swapped $LolA^{F68E}$ (published F47E)
337 [41,42] structure, supports the idea that the LolA monomeric structure around these sites is
338 intrinsically unstable. These findings also highlight the ease with which PLLLF proteins can
339 evolve strand-swapped dimerization. This finding, along with the grouping of both proteins into
340 the same superfamily by SCOP [74], also raises the intriguing possibility of a shared ancestry
341 between LolA and GerS. During the evolution of monoderm bacteria, which involved the loss of
342 the ancestral outer membrane [75–77], there would no longer be a need to transport
343 lipoproteins across the periplasmic space, facilitating a specialization of the ancestral proteins
344 during sporulation in endospore-forming monoderms [13,23]. This hypothesis may also clarify
345 why PLLLF proteins are absent in certain non-spore-forming monoderms such as
346 *Staphylococcus aureus* and the seemingly convergent roles of LppX [10] and Lpr proteins
347 [11,12] in transporting glycolipids across the mycobacterial periplasm.

348 Much work remains to be done to understand precisely why GerS strand swapping
349 stabilizes its interaction with CwlD. Notably, CwlD binding to its Zn^{2+} co-factor also stabilizes the
350 GerS:CwlD interaction, so it is possible that Zn^{2+}-bound CwlD adopts a conformation that

351 similarly promotes GerS strand-swapping. Identifying the allosteric circuit that allows GerS
352 binding to CwlD to be communicated to CwlD's active site and vice versa will likely provide
353 insight into the role of GerS strand-swapping in the allosteric activation of CwlD. Another
354 question that arises from our identification of GerS orthologs in other clostridial species that do
355 not form dimers is whether these GerS orthologs have additional or different conserved
356 functions beyond regulating CwlD activity during cortex modification? The requirement of CwlD
357 for GerS processing and incorporation into the spore may indicate that GerS functions in a very
358 specialized way in the Peptostreptococcaceae family [22]. In contrast, it is possible that GerS
359 orthologs in other Clostridia function similarly to SsdC in *B. subtilis*, which is required for proper
360 spore morphology through its impacts on spore cortex assembly [13]. Nevertheless, how these
361 orthologs are incorporated into the spore if they do not interact with CwlD as well as whether
362 GerS and CwlD can independently localize to the forespore remain open questions and will
363 require analyses in organisms other than *C. difficile*.
364
365 **Materials and Methods**
366
367 **Structural alignment, sequence analysis, and phylogenetics.** 17 PLLLF proteins were
368 selected from the InterPro [44] SuperFamily SSF89392, representing the taxonomic diversity of
369 the PLLLF protein family. AlphaFold3 [47] was used to predict the structure of each protein. The
370 17 proteins were aligned using DALI [48], which generates an amino-acid sequence alignment
371 based on the closest amino acids in each aligned structure. The structural alignment was imported
372 into Geneious Prime 2024.0.5. to calculate the %identity and %similarity between each sequence
373 (see Table S1). For %similarity calculations, the Blosum45 matrix was used with a threshold of 0.
374 WebLogo [78] was used to generate the sequence logo of the structural alignment.
375 The phylogenetic tree of the major bacterial classes, with Archaea and Eukarya as used
376 as outgroups, was constructed using genomes publicly available on KBase [79]. Five genomes

377 for each class were selected, although there were several instances when five were not available
378 for a given class. The complete list of these genomes can be found in Table S2. The KBase app
379 "Insert Genome into SpeciesTree - v2.2.0" was used to identify, concatenate, and align a set of
380 49 core, universal genes defined by COG (Clusters of Orthologous Groups) gene families across
381 all selected genomes. The app generates the phylogenetic tree using FastTree2 [80]. The tree
382 was visualized and prepared into a figure using iTOL [81]. Identification of PLLLF proteins in each
383 class was done by searching for PLLLF proteins encoded by members of each class in the
384 InterPro [44] SuperFamily SSF89392 and by running FoldSeek [43] using the LolA crystal
385 structure (1IWL).
386
387 **Bacterial strains and growth conditions.** *C. difficile* strains 630Δ*erm*Δ*cwlD*Δ*pyrE* and
388 630Δ*erm*Δ*gerS*Δ*pyrE* were used as the parental strains for *pyrE*-based allelic-coupled exchange
389 (ACE) [82], which allows for single-copy complementation from the ectopic *pyrE* locus. The *C.*
390 *difficile* strains used are listed in Table S3. They were grown on brain heart infusion media (BHIS)
391 supplemented with taurocholate (TA, 0.1% wt/vol; 1.9 mM), thiamphenicol (10-15 µg /mL),
392 kanamycin (50 µg/ml), cefoxitin (8 µg/ml) and L-cysteine (0.1% w/v; 8.25 mM) as needed. For
393 ACE, *C. difficile* was grown on *C. difficile* defined medium (CDDM) [83]. Cultures were grown at
394 37°C under anaerobic conditions using a gas mixture containing 85% N_2, 5% CO_2 and 10% H_2.
395 *Escherichia coli* strains used for BL21(DE3)-based protein production and HB101/pRK24-
396 based conjugations are listed in Table S3. *E. coli* strains were grown at 37°C with shaking at 225
397 rpm in Luria-Bertani broth (LB). The media was supplemented with chloramphenicol (20 µg/ml),
398 ampicillin (50 µg/ml), or kanamycin (30 µg/ml) as indicated.

399 ***E. coli* strain construction.** Plasmid constructs were confirmed by sequencing using Genewiz
400 or Plasmidsaurus (see the Benchling links in Table S3) and transformed into either the
401 HB101/pRK24 conjugation strain (used with *C. difficile*) or BL21(DE3) expression strain.

402 ***C. difficile* strain construction and complementation**. Allele-couple exchange (ACE) was used
403 to construct all complementation strains as previously described by conjugating HB101/ pRK24
404 carrying pMTL-YN1C plasmids into Δ*pyrE*-based strains.
405
406 **Protein purification.** Starter cultures were grown in 20 mL LB broth with 30 µg/mL of
407 kanamycin and, in some cases, 100 µg/mL ampicillin. Terrific broth (TB) with ampicillin and
408 kanamycin was inoculated with the starter culture (1:1000) and incubated for ~60 hr at 20°C
409 with 225 rpm shaking. The purifications were carried out in two steps: nickel bead-based (co-
410)affinity purification followed by size exclusion chromatography (SEC). Affinity purification was
411 carried out as stated above: the cells were pelleted, resuspended in lysis buffer (500 mM NaCl,
412 50 mM Tris [pH 7.5], 15 mM imidazole, 10% [vol/vol] glycerol, 2 mM ß-mercaptoethanol), flash
413 frozen in liquid nitrogen, thawed and then sonicated. The insoluble material was pelleted, and
414 the soluble fraction was incubated with Ni-NTA agarose beads (Qiagen) for 2 hours to capture
415 the His_6-tagged proteins. Washes were carried out five times with low imidazole buffer (500mM
416 NaCl, 10mM Tris-HCl pH 7.5, 10% (v/v) glycerol, 15 mM imidazole, 2 mM ß -mercaptoethanol)
417 to decrease non-specific binding to the beads. Proteins were eluted using high-imidazole buffer
418 (500 mM NaCl, 50 mM Tris [pH 7.5], 200 mM imidazole, 10% [vol/vol] glycerol, 2 mM ß-
419 mercaptoethanol) after nutating the sample for 5 to 10 min. Pooled protein elutions were
420 concentrated to 20 mg/ml or less in a size exclusion chromatography buffer consisting of 200
421 mM NaCl, 10 mM Tris HCl pH 7.5, 5% glycerol, and 1 mM DTT.

422 **Size exclusion chromatography (SEC**). SEC was carried out using a Superdex 200 Increase
423 10/300 GL (GE Healthcare) column. A high-resolution protocol was used to resolve affinity-
424 purified protein elutions by SEC. Specifically, purified proteins were diluted to a final
425 concentration of 10 mg/mL in the SEC buffer listed above, and then 100 µL of the 10 mg/mL
426 diluted protein was resolved using a 0.2 mL/min flow rate. The resulting fractions were resolved

427 using SDS-PAGE, and the gels were Coomassie stained using GelCode Blue according to the
428 manufacturer's instructions (ThermoFisher Scientific). Protein sequencing of non-GerS bands
429 was performed by automated Edman degradation on an ABI Procise 494 HT Protein/Peptide
430 Sequencer at the Tufts University Core Facility (TUCF).

431 **Western blot analysis.** Samples for immunoblotting were prepared by resuspending sporulating
432 cell pellets in 100 µl of PBS, and freeze-thawing a 50 µL aliquot of this resuspension for three
433 cycles. The pellet was then resuspended in 100 µL EBB buffer (8 M urea, 2 M thiourea, 4% [wt/vol]
434 SDS, 2% [vol/vol] ß-mercaptoethanol). *C. difficile* spores (~1 x 10^6) were resuspended in EBB
435 buffer, which extracts proteins in all layers of the spore, including the core. Both sporulating cells
436 and spores were incubated at 95°C for 20 min with vortex mixing. Samples were centrifuged for
437 5 min at 15,000 rpm, and 4 x sample buffer (40% [vol/vol] glycerol, 1 M Tris [pH 6.8], 20% [vol/vol]
438 ß-mercaptoethanol, 8% [wt/vol] SDS, 0.04% [wt/vol] bromophenol blue) was added. Samples
439 were incubated again at 95°C for 5 to 10 min with vortex mixing followed by centrifugation for 5
440 min at 15,000 rpm. The samples were resolved by the use of 14% SDS-PAGE gels and
441 transferred to a Millipore Immobilon-FL polyvinylidene difluoride (PVDF) membrane. The
442 membranes were blocked in Odyssey blocking buffer with 0.1% (vol/vol) Tween 20. Polyclonal
443 rabbit anti-GerS and anti-CwlD antibodies were used at a 1:500 and 1:750 dilution, respectively.
444 Polyclonal mouse anti-SleC antibodies were used at a 1:5000 dilution. IRDye 680CW and 800CW
445 infrared dye-conjugated secondary antibodies were used at 1:30,000 dilutions. An Odyssey LiCor
446 CLx was used to visualize secondary antibody infrared fluorescence emissions.
447

448 **Spore purification.** Sporulation was induced on 70:30 agar plates for 3-5 days, and the cultures
449 were harvested for spore purifications. Spores were washed 6 times in ice-cold water, incubated
450 overnight in water on ice, treated with DNase I (New England Biolabs) at 37°C for 60 min, and
451 purified on a HistoDenz (Sigma- Aldrich) gradient. Phase-contrast microscopy was used to assess

452 spore purity (>95% pure); the optical density of the spore stock was measured at OD_{600}; and
453 spores were stored in water at 4°C. Four 70:30 plates were used to induce sporulation for each
454 strain; purified spores were resuspended in 200 µL, and the total optical density of this mixture
455 was determined for each strain. At least three independent spore preparations were performed.
456 Spore purity as assessed by phase-contrast microscopy. Only spore suspensions that were >95%
457 pure were used.
458

459 **Optical density-based germination assay.** For OD_{600}-based germination assays, germination
460 was induced with taurocholate in 96-well plates. Specifically, ~1.6 x 10^7 spores (0.55 OD_{600} units)
461 for each condition tested were resuspended in BHIS and then 180 µL of this suspension was
462 aliquoted in duplicate into a 96 well flat-bottom tissue culture plate (Falcon) for each condition
463 tested. The spores were exposed to 1% taurocholate (19 mM), or water (untreated) in a final
464 volume of 200 µL. The OD_{600} of the sample was measured every 3 minutes in a Synergy H1
465 microplate reader (Biotek) at 37℃ with constant shaking between readings. The change in OD_{600}
466 over time was calculated as the ratio of the OD_{600} at each time point to the OD_{600} at time zero.
467 Relative germination was calculated by measuring the area between the drop in OD_{600} and 1.0
468 after 39 minutes (13 reads). These assays were performed on 3-6 independent spore
469 preparations depending on the condition. Data shown are averages from these replicates.
470 Comparison of each mean to WT was performed using a one-way ANOVA followed by Dunnett's
471 multiple comparisons test, with a single-pooled variance.
472
473

References

[1] A. De Las Peñas, L. Connolly, C.A. Gross, The σE-mediated response to extracytoplasmic stress in *Escherichia coli* is transduced by RseA and RseB, two negative regulators of σE, Mol Microbiol 24 (1997) 373–385. https://doi.org/10.1046/J.1365-2958.1997.3611718.X.

[2] M.J. Schurr, H. Yu, J.M. Martinez-Salazar, J.C. Boucher, V. Deretic, Control of AlgU, a member of the sigma E-like family of stress sigma factors, by the negative regulators MucA and MucB and *Pseudomonas aeruginosa* conversion to mucoidy in cystic fibrosis, J Bacteriol 178 (1996) 4997–5004. https://doi.org/10.1128/JB.178.16.4997-5004.1996.

[3] D. Jaiman, R. Nagampalli, K. Persson, A comparative analysis of lipoprotein transport proteins: LolA and LolB from *Vibrio cholerae* and LolA from *Porphyromonas gingivalis*, Scientific Reports 2023 13:1 13 (2023) 1–10. https://doi.org/10.1038/s41598-023-33705-y.

[4] S. Okuda, H. Tokuda, Model of mouth-to-mouth transfer of bacterial lipoproteins through inner membrane LolC, periplasmic LolA, and outer membrane LolB, Proc Natl Acad Sci U S A 106 (2009) 5877–5882. https://doi.org/10.1073/PNAS.0900896106/SUPPL_FILE/0900896106SI.PDF.

[5] V. Furlanetto, C. Divne, LolA and LolB from the plant-pathogen *Xanthomonas campestris* forms a stable heterodimeric complex in the absence of lipoprotein, Front Microbiol 14 (2023) 1216799. https://doi.org/10.3389/FMICB.2023.1216799/BIBTEX.

[6] K.L. May, M. Grabowicz, Outer membrane lipoproteins: late to the party, but the center of attention, J Bacteriol (2024). https://doi.org/10.1128/JB.00442-24.

[7] E.D. LoVullo, L.F. Wright, V. Isabella, J.F. Huntley, M.S. Pavelka, Revisiting the gram-negative lipoprotein paradigm, J Bacteriol 197 (2015) 1705–1715. https://doi.org/10.1128/JB.02414-14/SUPPL_FILE/ZJB999093599SO4.XLSX.

[8] S. ichiro Narita, H. Tokuda, Sorting of bacterial lipoproteins to the outer membrane by the Lol system, Methods Mol Biol 619 (2010) 117–129. https://doi.org/10.1007/978-1-60327-412-8_7.

[9] S.Y. Tanaka, S.I. Narita, H. Tokuda, Characterization of the *Pseudomonas aeruginosa* Lol system as a lipoprotein sorting mechanism, Journal of Biological Chemistry 282 (2007) 13379–13384. https://doi.org/10.1074/jbc.M611840200.

[10] G. Sulzenbacher, S. Canaan, Y. Bordat, O. Neyrolles, G. Stadthagen, V. Roig-Zamboni, J. Rauzier, D. Maurin, F. Laval, M. Daffé, C. Cambillau, B. Gicquel, Y. Bourne, M. Jackson, LppX is a lipoprotein required for the translocation of phthiocerol dimycocerosates to the surface of *Mycobacterium tuberculosis*, EMBO Journal 25 (2006) 1436–1444. https://doi.org/10.1038/SJ.EMBOJ.7601048/SUPPL_FILE/EMBJ7601048-SUP-0001.PDF.

[11] M.G. Drage, H.C. Tsai, N.D. Pecora, T.Y. Cheng, A.R. Arida, S. Shukla, R.E. Rojas, C. Seshadri, D.B. Moody, W.H. Boom, J.C. Sacchettini, C. V. Harding, *Mycobacterium tuberculosis* lipoprotein LprG (Rv1411c) binds triacylated glycolipid agonists of Toll-like receptor 2, Nature Structural & Molecular Biology 2010 17:9 17 (2010) 1088–1095. https://doi.org/10.1038/nsmb.1869.

513 [12] J.S. Kim, L. Jiao, J. Il Oh, N.C. Ha, Y.H. Kim, Crystal structure and functional implications
514 of LprF from *Mycobacterium tuberculosis* and *M. bovis*, Acta Crystallogr D Biol Crystallogr
515 70 (2014) 2619–2630. https://doi.org/10.1107/S1399004714016599.

516 [13] J. Luhur, H. Chan, B. Kachappilly, A. Mohamed, C. Morlot, M. Awad, D. Lyras, N. Taib, S.
517 Gribaldo, D.Z. Rudner, C.D.A. Rodrigues, A dynamic, ring-forming MucB / RseB-like
518 protein influences spore shape in *Bacillus subtilis*, PLoS Genet 16 (2020) e1009246.
519 https://doi.org/10.1371/JOURNAL.PGEN.1009246.

520 [14] K.A. Fimlaid, O. Jensen, M.L. Donnelly, M.B. Francis, J.A. Sorg, A. Shen, Identification of a
521 Novel Lipoprotein Regulator of *Clostridium difficile* Spore Germination, PLoS Pathog 11
522 (2015) e1005239. https://doi.org/10.1371/JOURNAL.PPAT.1005239.

523 [15] D.A. Burns, J.T. Heap, N.P. Minton, SleC is essential for germination of *Clostridium difficile*
524 spores in nutrient-rich medium supplemented with the bile salt taurocholate, J Bacteriol 192
525 (2010) 657–664. https://doi.org/10.1128/JB.01209-09/ASSET/F0B6A88D-0D10-4FE5-
526 ADDE-C2E652FF1E28/ASSETS/GRAPHIC/ZJB9990993070005.JPEG.

527 [16] D. Paredes-Sabja, P. Setlow, M.R. Sarker, SleC Is Essential for Cortex Peptidoglycan
528 Hydrolysis during Germination of Spores of the Pathogenic Bacterium *Clostridium*
529 *perfringens*, J Bacteriol 191 (2009) 2711–2720. https://doi.org/10.1128/JB.01832-08.

530 [17] D. Gutelius, K. Hokeness, S.M. Logan, C.W. Reid, Functional analysis of SleC from
531 *Clostridium difficile*: an essential lytic transglycosylase involved in spore germination,
532 Microbiology (N Y) 160 (2014) 209. https://doi.org/10.1099/MIC.0.072454-0.

533 [18] T. Fukushima, H. Yamamoto, A. Atrih, S.J. Foster, J. Sekiguchi, A polysaccharide
534 deacetylase gene (pdaA) is required for germination and for production of muramic δ-
535 lactam residues in the spore cortex of *Bacillus subtilis*, J Bacteriol 184 (2002) 6007–6015.
536 https://doi.org/10.1128/JB.184.21.6007-6015.2002/ASSET/281D2E2F-2AB6-4943-9460-
537 50EB1BA91E0B/ASSETS/GRAPHIC/JB2120422006.JPEG.

538 [19] H. Coullon, A. Rifflet, R. Wheeler, C. Janoir, I.G. Boneca, T. Candela, N-Deacetylases
539 required for muramic-lactam production are involved in *Clostridium difficile* sporulation,
540 germination, and heat resistance, Journal of Biological Chemistry 293 (2018) 18040–
541 18054. https://doi.org/10.1074/JBC.RA118.004273/ATTACHMENT/A0930DBF-1D55-
542 4CDE-96DE-AEFCB897DBF5/MMC1.ZIP.

543 [20] M.J. Tobin, S.Y. Cho, W. Profy, T.M. Ryan, D.H. Le, C. Lin, E.Z. Yip, J.L. Dorsey, B.R.
544 Levy, J.D. Rhodes, M.A. Welsh, Reconstituting Spore Cortex Peptidoglycan Biosynthesis
545 Reveals a Deacetylase That Catalyzes Transamidation, (2023).
546 https://doi.org/10.1021/acs.biochem.3c00100.

547 [21] C. Kim, M. Lee, B.T. Birhanu, D. Hesek, M. Chang, S. Mobashery, Synthesis of Muramyl-δ-
548 Lactam in Spore Peptidoglycan of *Clostridioides difficile*, ChemBioChem 24 (2023)
549 e202300282. https://doi.org/10.1002/CBIC.202300282.

550 [22] O.R. Diaz, C. V. Sayer, D.L. Popham, A. Shen, *Clostridium difficile* Lipoprotein GerS Is
551 Required for Cortex Modification and Thus Spore Germination, MSphere 3 (2018).
552 https://doi.org/10.1128/MSPHERE.00205-18/SUPPL_FILE/SPH003182575SF7.TIF.

553 [23] C.A. Feliciano, B.E. Eckenroth, O.R. Diaz, S. Doublié, A. Shen, A lipoprotein allosterically
554 activates the CwlD amidase during *Clostridioides difficile* spore formation, PLoS Genet 17
555 (2021) e1009791. https://doi.org/10.1371/JOURNAL.PGEN.1009791.

556 [24] P.R. Gouldson, C.R. Snell, R.P. Bywater, C. Higgs, C.A. Reynolds, Domain swapping in G-
557 protein coupled receptor dimers., Protein Engineering, Design and Selection 11 (1998)
558 1181–1193. https://doi.org/10.1093/PROTEIN/11.12.1181.

559 [25] L. Vitagliano, S. Adinolfi, F. Sica, A. Merlino, A. Zagari, L. Mazzarella, A potential allosteric
560 subsite generated by domain swapping in bovine seminal ribonuclease, J Mol Biol 293
561 (1999) 569–577. https://doi.org/10.1006/JMBI.1999.3158.

562 [26] R. Janowski, M. Kozak, E. Jankowska, Z. Grzonka, A. Grubb, M. Abrahamson, M.
563 Jaskolski, Human cystatin C, an amyloidogenic protein, dimerizes through three-
564 dimensional domain swapping, Nature Structural Biology 2001 8:4 8 (2001) 316–320.
565 https://doi.org/10.1038/86188.

566 [27] A.D. Cameron, B. Olin, M. Ridderström, B. Mannervik, T.A. Jones, Crystal structure of
567 human glyoxalase I—evidence for gene duplication and 3D domain swapping, EMBO J 16
568 (1997) 3386–3395. https://doi.org/10.1093/EMBOJ/16.12.3386.

569 [28] J. Vendome, S. Posy, X. Jin, F. Bahna, G. Ahlsen, L. Shapiro, B. Honig, Molecular design
570 principles underlying β-strand swapping in the adhesive dimerization of cadherins, Nature
571 Structural & Molecular Biology 2011 18:6 18 (2011) 693–700.
572 https://doi.org/10.1038/nsmb.2051.

573 [29] F. Rousseau, J.W.H. Schymkowitz, H.R. Wilkinson, L.S. Itzhaki, Three-dimensional domain
574 swapping in p13suc1 occurs in the unfolded state and is controlled by conserved proline
575 residues, Proceedings of the National Academy of Sciences 98 (2001) 5596–5601.
576 https://doi.org/10.1073/PNAS.101542098.

577 [30] K. Shivaji Paithankar, M. Enderle, D.C. Wirthensohn, A. Miller, M. Schlesner, F. Pfeiffer, A.
578 Rittner, M. Grininger, D. Oesterhelt, Structure of the archaeal chemotaxis protein CheY in a
579 domain-swapped dimeric conformation, (n.d.).
580 https://doi.org/10.1107/S2053230X19010896.

581 [31] M.J. Bennett, S. Choe, D. Eisenberg, Domain swapping: Entangling alliances between
582 proteins, Proc Natl Acad Sci U S A 91 (1994) 3127–3131.
583 https://doi.org/10.1073/PNAS.91.8.3127;WEBSITE:WEBSITE:PNAS-
584 SITE;WGROUP:STRING:PUBLICATION.

585 [32] N.M. Mascarenhas, S. Gosavi, Understanding protein domain-swapping using structure-
586 based models of protein folding, Prog Biophys Mol Biol 128 (2016) 113.
587 https://doi.org/10.1016/J.PBIOMOLBIO.2016.09.013.

588 [33] B. Brumshtein, S.R. Esswein, M. Landau, C.M. Ryan, J.P. Whitelegge, M.L. Phillips, D.
589 Cascio, M.R. Sawaya, D.S. Eisenberg, Formation of Amyloid Fibers by Monomeric Light
590 Chain Variable Domains, Journal of Biological Chemistry 289 (2014) 27513–27525.
591 https://doi.org/10.1074/JBC.M114.585638.

[34] B. Gerhartz, I. Ekiel, M. Abrahamson, Two stable unfolding intermediates of the disease-causing L68Q variant of human cystatin C, Biochemistry 37 (1998) 17309–17317. https://doi.org/10.1021/BI980873U/ASSET/IMAGES/LARGE/BI980873UF00007.JPEG.

[35] E. Zerovnik, V. Stoka, A. Mirtič, G. Gunčar, J. Grdadolnik, R.A. Staniforth, D. Turk, V. Turk, Mechanisms of amyloid fibril formation–focus on domain-swapping, Wiley Online Library 278 (2011) 2263–2282. https://doi.org/10.1111/J.1742-4658.2011.08149.X.

[36] M.J.-A.B. Polonica, undefined 2001, 3D domain swapping, protein oligomerization, and amyloid formation., Frontierspartnerships.Org 48 (2001) 807–827. https://doi.org/10.18388/ABP.2001_3849/PDF.

[37] P. Jurczak, P. Groves, A. Szymanska, S. Rodziewicz-Motowidlo, Human cystatin C monomer, dimer, oligomer, and amyloid structures are related to health and disease, FEBS Lett 590 (2016) 4192–4201. https://doi.org/10.1002/1873-3468.12463;WEBSITE:WEBSITE:FEBS;PAGE:STRING:ARTICLE/CHAPTER.

[38] J.H. Ha, J.M. Karchin, N. Walker-Kopp, C.A. Castañeda, S.N. Loh, Engineered domain swapping as an on/off switch for protein function, Chem Biol 22 (2015) 1384–1393. https://doi.org/10.1016/j.chembiol.2015.09.007.

[39] J.M. Modenbach, C. Möller, S. Asgarbeik, N. Geist, N. Rimkus, M. Dörr, H. Wolfgramm, L. Steil, A. Susemihl, L. Graf, O. Schmöker, D. Böttcher, E. Hammer, J. Glaubitz, M. Lammers, M. Delcea, U. Völker, A.A. Aghdassi, M.M. Lerch, F.U. Weiss, U.T. Bornscheuer, M. Sendler, Biochemical analyses of cystatin-C dimers and cathepsin-B reveals a trypsin-driven feedback mechanism in acute pancreatitis, Nature Communications 2025 16:1 16 (2025) 1–18. https://doi.org/10.1038/s41467-025-56875-x.

[40] S. Posy, L. Shapiro, B. Honig, Sequence and structural determinants of strand swapping in cadherin domains: Do all cadherins bind through the same adhesive interface?, J Mol Biol 378 (2008) 954. https://doi.org/10.1016/J.JMB.2008.02.063.

[41] A. Miyamoto, S. ichi Matsuyama, H. Tokuda, Dominant negative mutant of a lipoprotein-specific molecular chaperone, LolA, tightly associates with LolCDE, FEBS Lett 528 (2002) 193–196. https://doi.org/10.1016/S0014-5793(02)03305-7.

[42] E. Kaplan, N.P. Greene, A. Crow, V. Koronakis, Insights into bacterial lipoprotein trafficking from a structure of LolA bound to the LolC periplasmic domain, Proc Natl Acad Sci U S A 115 (2018) E7389–E7397. https://doi.org/10.1073/PNAS.1806822115/SUPPL_FILE/PNAS.1806822115.SM03.MOV.

[43] M. van Kempen, S.S. Kim, C. Tumescheit, M. Mirdita, J. Lee, C.L.M. Gilchrist, J. Söding, M. Steinegger, Fast and accurate protein structure search with Foldseek, Nature Biotechnology 2023 42:2 42 (2023) 243–246. https://doi.org/10.1038/s41587-023-01773-0.

[44] M. Blum, A. Andreeva, L. Cavalcanti Florentino, S. Rocio Chuguransky, T. Grego, E. Hobbs, B. Lazaro Pinto, A. Orr, T. Pa ysan-Laf osse, I. Ponamareva, G.A. Salazar, N. Bordin, P. eer Bor, A. Br idg, L. Colw ell, J. Gough, D.H. Haft, I. Letunic, F. Llinares-López, A. Marchler-Bauer, L. Meng-Papaxanthos, H. Mi, D.A. Natale, C.A. Orengo, A.P. Pandur ang an, D. Pio esan, C. ine Rivoire, C.J. istian Sigr ist, N. mada Thanki, F. ançoise Thibaud-Nissen, P.D. Thomas, S.C. Tosatto, C.H. W, A. Bat eman, InterPro: the protein

633 sequence classification resource in 2025, Nucleic Acids Res 1 (2013) 13–14.
634 https://doi.org/10.1093/NAR/GKAE1082.

635 [45] C. Camacho, G. Coulouris, V. Avagyan, N. Ma, J. Papadopoulos, K. Bealer, T.L. Madden,
636 BLAST+: Architecture and applications, BMC Bioinformatics 10 (2009) 1–9.
637 https://doi.org/10.1186/1471-2105-10-421/FIGURES/4.

638 [46] S.F. Altschul, W. Gish, W. Miller, E.W. Myers, D.J. Lipman, Basic local alignment search
639 tool, J Mol Biol 215 (1990) 403–410. https://doi.org/10.1016/S0022-2836(05)80360-2.

640 [47] J. Abramson, J. Adler, J. Dunger, R. Evans, T. Green, A. Pritzel, O. Ronneberger, L.
641 Willmore, A.J. Ballard, J. Bambrick, S.W. Bodenstein, D.A. Evans, C.C. Hung, M. O'Neill,
642 D. Reiman, K. Tunyasuvunakool, Z. Wu, A. Žemgulytė, E. Arvaniti, C. Beattie, O. Bertolli,
643 A. Bridgland, A. Cherepanov, M. Congreve, A.I. Cowen-Rivers, A. Cowie, M. Figurnov, F.B.
644 Fuchs, H. Gladman, R. Jain, Y.A. Khan, C.M.R. Low, K. Perlin, A. Potapenko, P. Savy, S.
645 Singh, A. Stecula, A. Thillaisundaram, C. Tong, S. Yakneen, E.D. Zhong, M. Zielinski, A.
646 Žídek, V. Bapst, P. Kohli, M. Jaderberg, D. Hassabis, J.M. Jumper, Accurate structure
647 prediction of biomolecular interactions with AlphaFold 3, Nature 2024 630:8016 630 (2024)
648 493–500. https://doi.org/10.1038/s41586-024-07487-w.

649 [48] L. Holm, A. Laiho, P. Törönen, M. Salgado, DALI shines a light on remote homologs: One
650 hundred discoveries, Protein Science 32 (2023) e4519. https://doi.org/10.1002/PRO.4519.

651 [49] K. Remans, K. Pauwels, P. van Ulsen, L. Buts, P. Cornelis, J. Tommassen, S.N. Savvides,
652 K. Decanniere, P. Van Gelder, Hydrophobic Surface Patches on LolA of *Pseudomonas*
653 *aeruginosa* Are Essential for Lipoprotein Binding, J Mol Biol 401 (2010) 921–930.
654 https://doi.org/10.1016/J.JMB.2010.06.067.

655 [50] K. Takeda, H. Miyatake, N. Yokota, S.I. Matsuyama, H. Tokuda, K. Miki, Crystal structures
656 of bacterial lipoprotein localization factors, LolA and LolB, EMBO J 22 (2003) 3199–3209.
657 https://doi.org/10.1093/EMBOJ/CDG324.

658 [51] J. Botas, Á. Rodríguez Del Río, J. Giner-Lamia, J. Huerta-Cepas, GeCoViz: genomic
659 context visualisation of prokaryotic genes from a functional and evolutionary perspective,
660 Nucleic Acids Res 50 (2022) W352–W357. https://doi.org/10.1093/NAR/GKAC367.

661 [52] J. Herson, M. Krummenacker, A. Spaulding, P. O'Maille, P.D. Karp, The Genome Explorer
662 genome browser, MSystems 9 (2024). https://doi.org/10.1128/MSYSTEMS.00267-
663 24/ASSET/D092CD98-EDF4-4F91-B5B5-
664 0333B26B6D93/ASSETS/IMAGES/LARGE/MSYSTEMS.00267-24.F007.JPG.

665 [53] E.C. Meng, T.D. Goddard, E.F. Pettersen, G.S. Couch, Z.J. Pearson, J.H. Morris, T.E.
666 Ferrin, UCSF ChimeraX: Tools for structure building and analysis, Protein Science 32
667 (2023) e4792. https://doi.org/10.1002/PRO.4792.

668 [54] S. Bello, S. McQuay, B. Rudra, R.S. Gupta, Robust demarcation of the family
669 Peptostreptococcaceae and its main genera based on phylogenomic studies and taxon-
670 specific molecular markers, Int J Syst Evol Microbiol 74 (2024) 006247.
671 https://doi.org/10.1099/IJSEM.0.006247/CITE/REFWORKS.

672 [55] J.W. O'Neill, D.E. Kim, K. Johnsen, D. Baker, K.Y.J. Zhang, Single-site mutations induce
673 3D domain swapping in the B1 domain of Protein L from *Peptostreptococcus magnus*,

674 Structure 9 (2001) 1017–1027. https://doi.org/10.1016/S0969-2126(01)00667-
675 0/ASSET/72670EC8-3DCE-47A6-B0BE-0F27AFC6C8EF/MAIN.ASSETS/FX3.JPG.

676 [56] K.H. Miller, J.R. Karr, S. Marqusee, A Hinge Region cis-Proline in Ribonuclease A Acts as
677 a Conformational Gatekeeper for C-Terminal Domain Swapping, J Mol Biol 400 (2010)
678 567–578. https://doi.org/10.1016/J.JMB.2010.05.017.

679 [57] M. Orlikowska, E. Jankowska, R. Kołodziejczyk, M. Jaskólski, A. Szymańska, Hinge-loop
680 mutation can be used to control 3D domain swapping and amyloidogenesis of human
681 cystatin C, J Struct Biol 173 (2011) 406–413. https://doi.org/10.1016/J.JSB.2010.11.009.

682 [58] G. Calloni, T. Chen, S.M. Schermann, H.C. Chang, P. Genevaux, F. Agostini, G.G.
683 Tartaglia, M. Hayer-Hartl, F.U. Hartl, DnaK Functions as a Central Hub in the *E. coli*
684 Chaperone Network, Cell Rep 1 (2012) 251–264.
685 https://doi.org/10.1016/j.celrep.2011.12.007.

686 [59] M. Kovermann, F.X. Schmid, J. Balbach, Molecular function of the prolyl cis/trans
687 isomerase and metallochaperone SlyD, Biol Chem 394 (2013) 965–975.
688 https://doi.org/10.1515/HSZ-2013-0137/ASSET/GRAPHIC/HSZ-2013-0137_CV3.JPG.

689 [60] S. Hottenrott, T. Schumann, A. Plückthun, G. Fischer, J.U. Rahfeld, The *Escherichia coli*
690 SlyD is a metal ion-regulated peptidyl-prolyl cis/trans-isomerase, Journal of Biological
691 Chemistry 272 (1997) 15697–15701. https://doi.org/10.1074/jbc.272.25.15697.

692 [61] A. Chikunova, M.P. Manley, C.N. Heijjer, C.S. Drenth, A.J. Cramer-Blok, M.U.D. Ahmad, A.
693 Perrakis, M. Ubbink, Conserved proline residues prevent dimerization and aggregation in
694 the β-lactamase BlaC, Protein Science 33 (2024) e4972.
695 https://doi.org/10.1002/PRO.4972.

696 [62] H. Fu, G.R. Grimsley, A. Razvi, J.M. Scholtz, C.N. Pace, Increasing protein stability by
697 improving beta-turns, Proteins: Structure, Function, and Bioinformatics 77 (2009) 491–498.
698 https://doi.org/10.1002/PROT.22509.

699 [63] C.M. Wilmot, J.M. Thornton, Analysis and prediction of the different types of β-turn in
700 proteins, J Mol Biol 203 (1988) 221–232. https://doi.org/10.1016/0022-2836(88)90103-9.

701 [64] E.G. Hutchinson, J.M. Thornton, A revised set of potentials for β-turn formation in proteins,
702 Protein Science 3 (1994) 2207–2216. https://doi.org/10.1002/PRO.5560031206.

703 [65] M.W. MacArthur, J.M. Thornton, Influence of proline residues on protein conformation, J
704 Mol Biol 218 (1991) 397–412. https://doi.org/10.1016/0022-2836(91)90721-H.

705 [66] N. Nandwani, P. Surana, H. Negi, N.M. Mascarenhas, J.B. Udgaonkar, R. Das, S. Gosavi,
706 A five-residue motif for the design of domain swapping in proteins, Nature Communications
707 2019 10:1 10 (2019) 1–13. https://doi.org/10.1038/s41467-019-08295-x.

708 [67] F. Ding, K.C. Prutzman, S.L. Campbell, N. V. Dokholyan, Topological determinants of
709 protein domain swapping, Structure 14 (2006) 5–14.
710 https://doi.org/10.1016/J.STR.2005.09.008.

711 [68] J.W. O'Neill, D.E. Kim, K. Johnsen, D. Baker, K.Y.J. Zhang, Single-site mutations induce
712 3D domain swapping in the B1 domain of Protein L from *Peptostreptococcus magnus*,

Structure 9 (2001) 1017–1027. https://doi.org/10.1016/S0969-2126(01)00667-0/ASSET/72670EC8-3DCE-47A6-B0BE-0F27AFC6C8EF/MAIN.ASSETS/FX3.JPG.

[69] A. Cámara-Artigas, S. Martínez-Rodríguez, E. Ortiz-Salmerón, J.M. Martín-García, 3D domain swapping in a chimeric c-Src SH3 domain takes place through two hinge loops, J Struct Biol 186 (2014) 195–203. https://doi.org/10.1016/J.JSB.2014.02.007.

[70] A. Szymánska, E. Jankowska, M. Orlikowska, I. Behrendt, P. Czaplewska, S. Rodziewicz-Motowidło, Influence of point mutations on the stability, dimerization, and oligomerization of human cystatin C and its L68Q variant, Front Mol Neurosci 5 (2012) 82–82. https://doi.org/10.3389/FNMOL.2012.00082/PDF<IMG.

[71] M. Bergdoll, M. Remy, C. Cagnon, J.M.- Structure, undefined 1997, Proline-dependent oligomerization with arm exchange, Cell.ComM Bergdoll, MH Remy, C Cagnon, JM Masson, P DumasStructure, 1997•cell.Com (n.d.). https://www.cell.com/AJHG/fulltext/S0969-2126(97)00196-2 (accessed May 14, 2025).

[72] A. Di Donate, V. Cafaro, G. D'Alessio, Ribonuclease A can be transformed into a dimeric ribonuclease with antitumor activity, Journal of Biological Chemistry 269 (1994) 17394–17396. https://doi.org/10.1016/S0021-9258(17)32451-1.

[73] F.U. Battistuzzi, A. Feijao, S.B. Hedges, A genomic timescale of prokaryote evolution: Insights into the origin of methanogenesis, phototrophy, and the colonization of land, BMC Evol Biol 4 (2004). https://doi.org/10.1186/1471-2148-4-44,.

[74] T.J.P. Hubbard, A.G. Murzin, S.E. Brenner, C. Chothia, SCOP: A Structural Classification of Proteins database, Nucleic Acids Res 25 (1997) 236–239. https://doi.org/10.1093/NAR/25.1.236,.

[75] D. Megrian, N. Taib, J. Witwinowski, C. Beloin, S. Gribaldo, One or two membranes? Diderm Firmicutes challenge the Gram-positive/Gram-negative divide, Mol Microbiol 113 (2020) 659–671. https://doi.org/10.1111/MMI.14469.

[76] N. Taib, D. Megrian, J. Witwinowski, P. Adam, D. Poppleton, G. Borrel, C. Beloin, S. Gribaldo, Genome-wide analysis of the Firmicutes illuminates the diderm/monoderm transition, Nature Ecology & Evolution 2020 4:12 4 (2020) 1661–1672. https://doi.org/10.1038/s41559-020-01299-7.

[77] J. Witwinowski, A. Sartori-Rupp, N. Taib, N. Pende, T.N. Tham, D. Poppleton, J.M. Ghigo, C. Beloin, S. Gribaldo, An ancient divide in outer membrane tethering systems in bacteria suggests a mechanism for the diderm-to-monoderm transition, Nature Microbiology 2022 7:3 7 (2022) 411–422. https://doi.org/10.1038/s41564-022-01066-3.

[78] G.E. Crooks, G. Hon, J.M. Chandonia, S.E. Brenner, WebLogo: A Sequence Logo Generator, Genome Res 14 (2004) 1188–1190. https://doi.org/10.1101/GR.849004.

[79] A.P. Arkin, R.W. Cottingham, C.S. Henry, N.L. Harris, R.L. Stevens, S. Maslov, P. Dehal, D. Ware, F. Perez, S. Canon, M.W. Sneddon, M.L. Henderson, W.J. Riehl, D. Murphy-Olson, S.Y. Chan, R.T. Kamimura, S. Kumari, M.M. Drake, T.S. Brettin, E.M. Glass, D. Chivian, D. Gunter, D.J. Weston, B.H. Allen, J. Baumohl, A.A. Best, B. Bowen, S.E. Brenner, C.C. Bun, J.M. Chandonia, J.M. Chia, R. Colasanti, N. Conrad, J.J. Davis, B.H. Davison, M. Dejongh, S. Devoid, E. Dietrich, I. Dubchak, J.N. Edirisinghe, G. Fang, J.P.

Faria, P.M. Frybarger, W. Gerlach, M. Gerstein, A. Greiner, J. Gurtowski, H.L. Haun, F. He, R. Jain, M.P. Joachimiak, K.P. Keegan, S. Kondo, V. Kumar, M.L. Land, F. Meyer, M. Mills, P.S. Novichkov, T. Oh, G.J. Olsen, R. Olson, B. Parrello, S. Pasternak, E. Pearson, S.S. Poon, G.A. Price, S. Ramakrishnan, P. Ranjan, P.C. Ronald, M.C. Schatz, S.M.D. Seaver, M. Shukla, R.A. Sutormin, M.H. Syed, J. Thomason, N.L. Tintle, D. Wang, F. Xia, H. Yoo, S. Yoo, D. Yu, KBase: The United States Department of Energy Systems Biology Knowledgebase, Nature Biotechnology 2018 36:7 36 (2018) 566–569. https://doi.org/10.1038/nbt.4163.

[80] M.N. Price, P.S. Dehal, A.P. Arkin, FastTree 2 – Approximately Maximum-Likelihood Trees for Large Alignments, PLoS One 5 (2010) e9490. https://doi.org/10.1371/JOURNAL.PONE.0009490.

[81] I. Letunic, P. Bork, Interactive Tree of Life (iTOL) v6: recent updates to the phylogenetic tree display and annotation tool, Nucleic Acids Res 52 (2024) W78–W82. https://doi.org/10.1093/NAR/GKAE268.

[82] Y.K. Ng, M. Ehsaan, S. Philip, M.M. Collery, C. Janoir, A. Collignon, S.T. Cartman, N.P. Minton, Expanding the Repertoire of Gene Tools for Precise Manipulation of the *Clostridium difficile* Genome: Allelic Exchange Using pyrE Alleles, PLoS One 8 (2013) e56051. https://doi.org/10.1371/JOURNAL.PONE.0056051.

[83] T. Karasawa, S. Ikoma, K. Yamakawa, S. Nakamura, A defined growth medium for *Clostridium difficile*, Microbiology (N Y) 141 (1995) 371–375. https://doi.org/10.1099/13500872-141-2-371,.

[84] M. Lauren Donnelly, W. Li, Y.Q. Li, L. Hinkel, P. Setlow, A. Shen, A *Clostridium difficile*-specific, gel-forming protein required for optimal spore germination, MBio 8 (2017). https://doi.org/10.1128/MBIO.02085-16,.

[85] R.A. Laskowski, J. Jabłońska, L. Pravda, R.S. Vařeková, J.M. Thornton, PDBsum: Structural summaries of PDB entries, Protein Science 27 (2018) 129–134. https://doi.org/10.1002/PRO.3289.

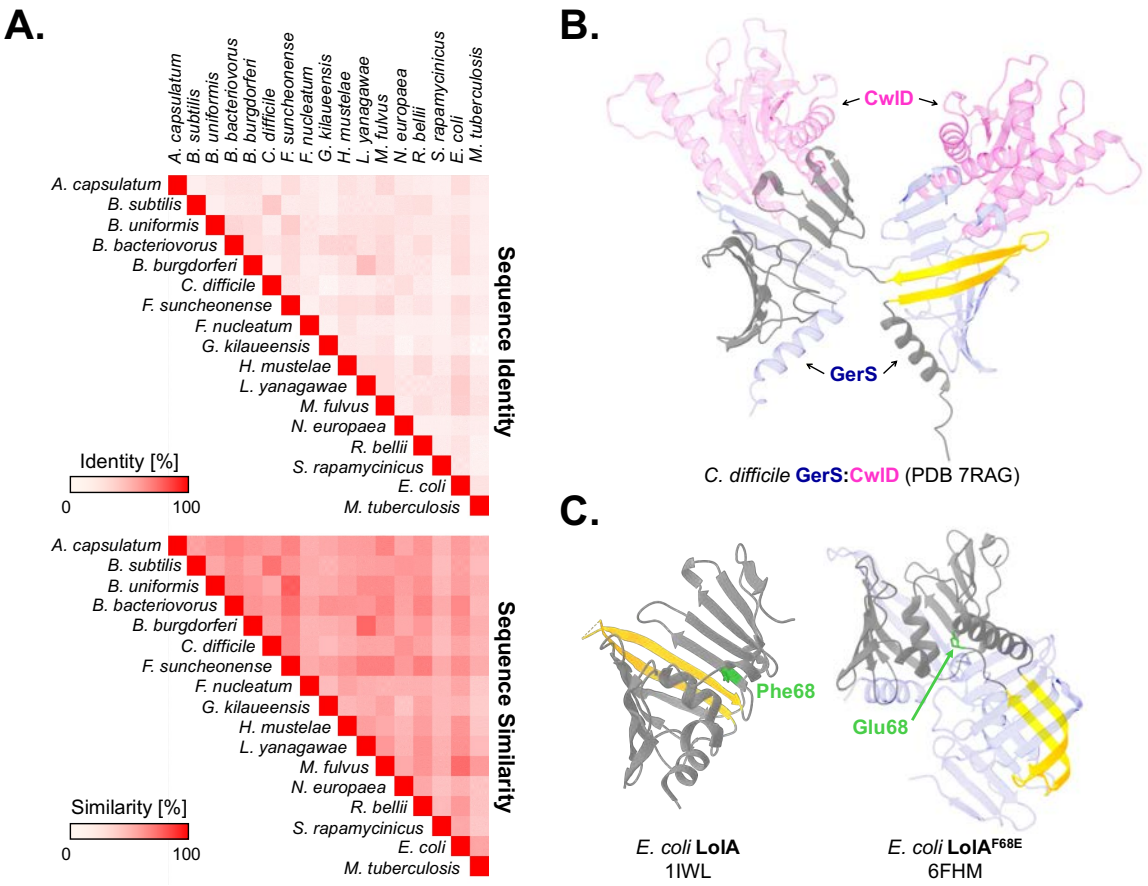

Figure 1. PLLLF proteins are structurally similar but share low sequence identity. A) Comparisons of sequence identity and sequence similarity between 17 representative PLLLF proteins. Gradients represent percentages from 0 to 100. B) Ribbon representation of the crystal structure of the GerS-CwlD complex (PBD 7RAG) with the GerS strand swap colored yellow. The other GerS is colored in transparent blue, and both CwlD proteins are colored in transparent pink. C) Ribbon representation of the crystal structures of the *Escherichia coli* $LolA^{WT}$ (PDB 1IWL) and $LolA^{F68E}$ (PDB 6FHM). The strand swap in $LolA^{F68E}$ structure is shown in yellow; the corresponding β-strand in $LolA^{WT}$ is shown in yellow. The other $LolA^{F68E}$ protomer in the homodimer is colored in transparent blue. Residue 68, which is a phenylalanine in $LolA^{WT}$ and a glutamate in $LolA^{F68E}$, is colored green.

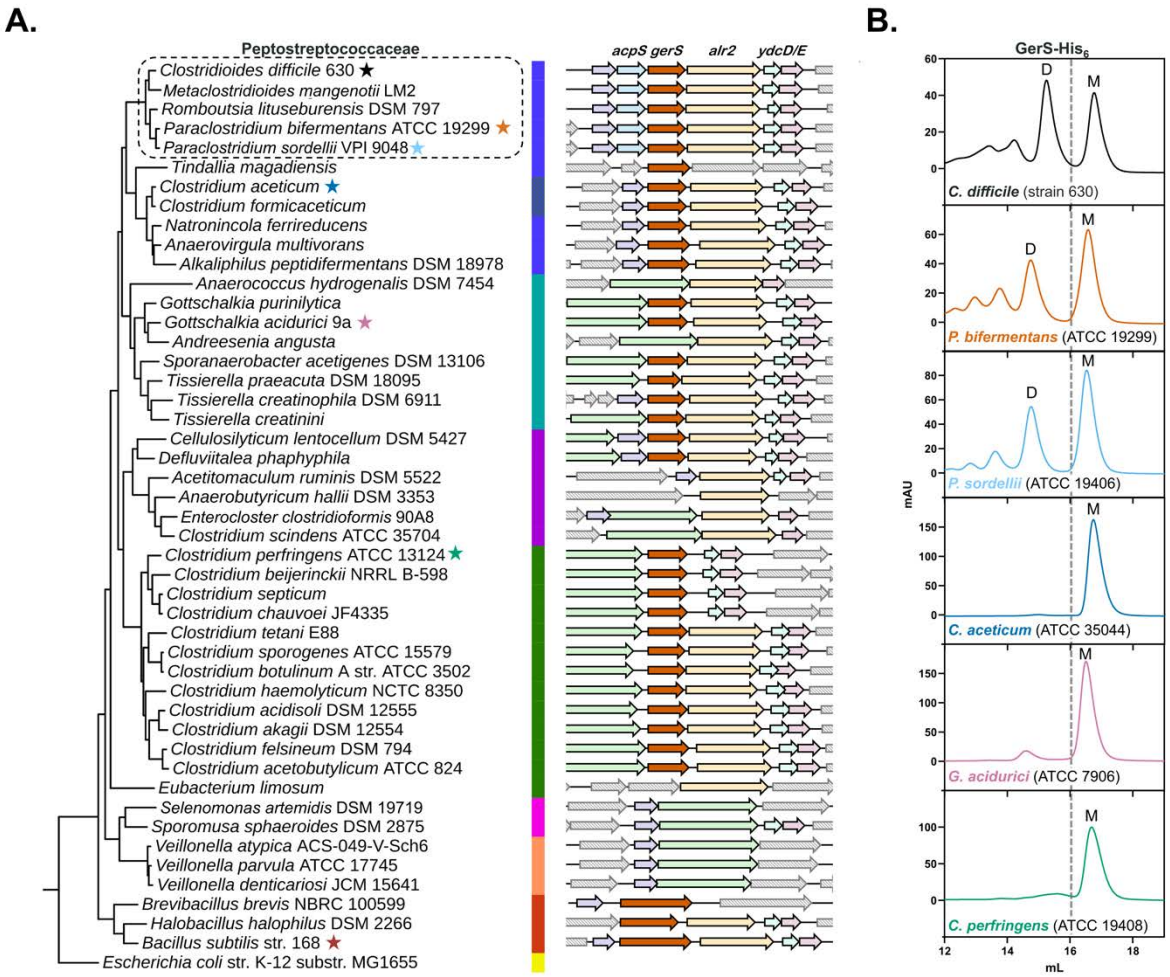

Figure 2. GerS dimerization is conserved in the Peptostreptococcaceae family despite being distributed throughout the Bacilliota phylum. A) Synteny analysis of the conserved *gerS* locus across the orders of the Bacilliota phylum. Peptostreptococcales (blue), Tissierelliales (turquoise), Lachnospirales (purple), Eubacterales (green), Selenomonadales (pink), Vellionellales (orange), Bacillales (red), and the outgroup Enterbacterales (yellow) classes are shown. Colored stars correspond to representative GerS orthologs selected for SEC analysis. B) Size exclusion chromatography (SEC) analysis of GerS orthologs tagged with His_6 for purification. Peaks are labeled with “D” for dimer or “M” for monomer.

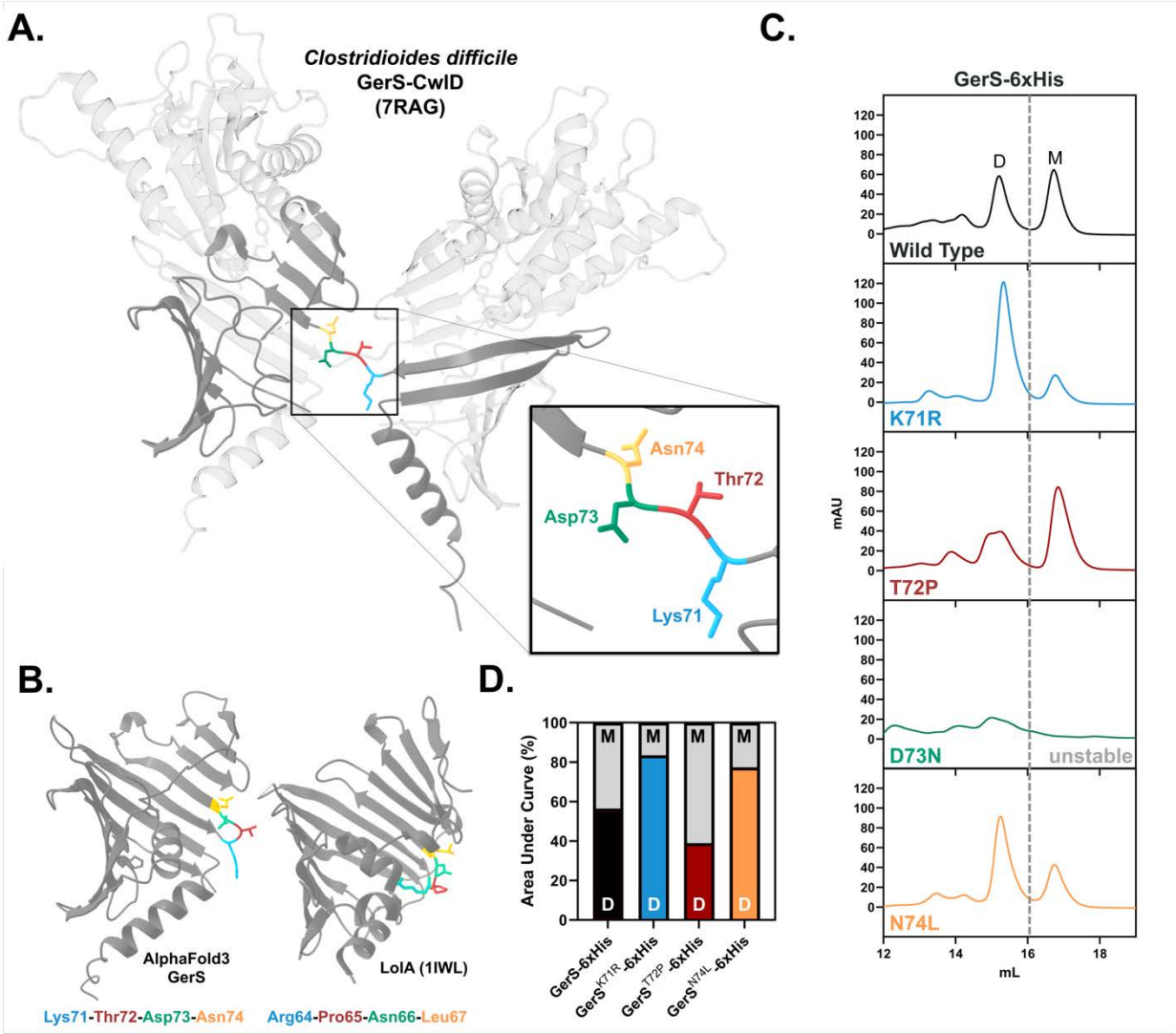

Figure 3. GerS hinge mutations guided by the LolA structure modulate its dimer:monomer equilibrium. A) Ribbon representation of the crystal structure of the GerS-CwlD complex (PDB 7RAG). The hinge is colored by the residue shown in the inset. B) Ribbon representation of the AlphaFold3 GerS structure and LolA crystal structure (PDB - 1IWL). Hinge of GerS and analogous residues on LolA are colored by aligned residues. C) Size exclusion chromatography (SEC) traces of each GerS variant tagged with His_6. Peaks are labeled with "D" for dimer or "M" for monomer. D) Ratio of the areas under each peak as a percentage of the total area measured. "D" is the area under the dimer peak, and "M" is the area under the monomer peak.

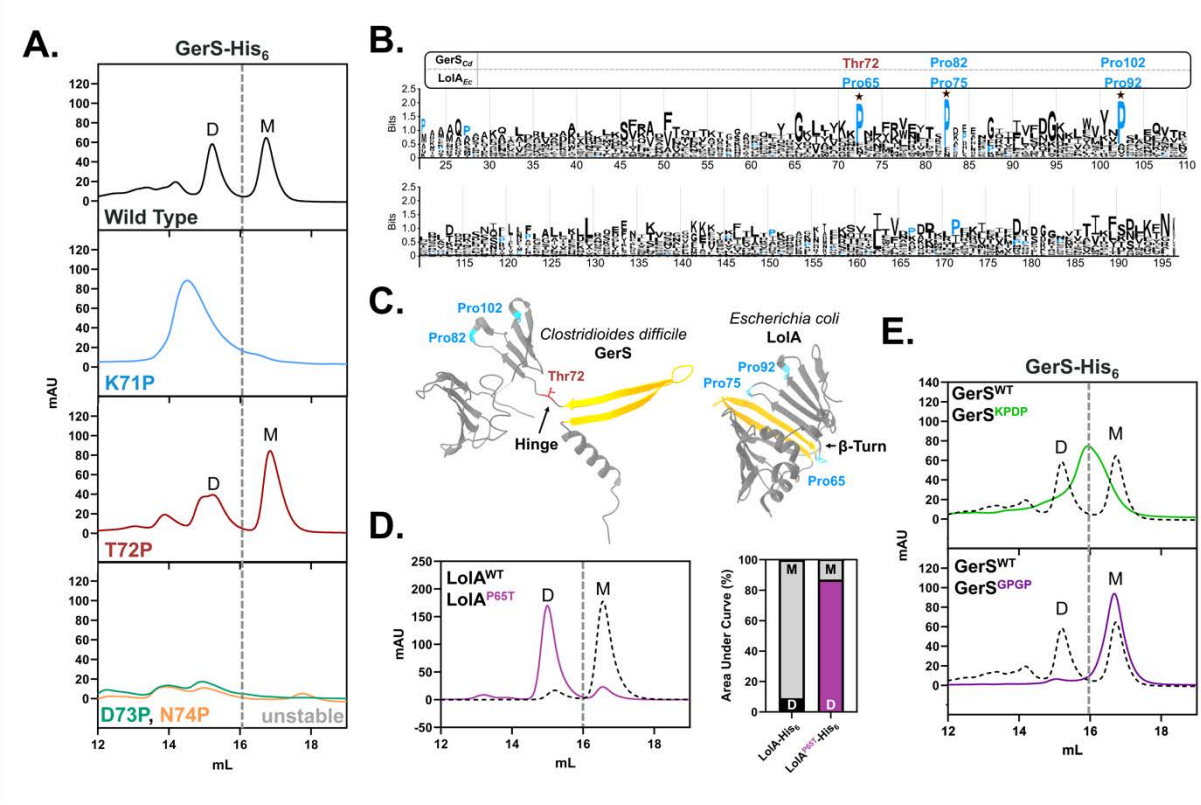

Figure 4. Prolines in the hinge region of PLLLF proteins reduce dimerization. A) Size exclusion chromatography (SEC) traces of His_6-tagged GerS variants carrying single proline substitutions in the hinge region. B) Sequence logo depicting the frequency of amino acids found at a given position based on DALI structural alignments of 17 representative PLLLF proteins [48]. Prolines are highlighted in blue. (C) Amino acids aligned to each conserved proline in GerS and LolA are displayed in the ribbon representations of the crystal structures shown (PDB 7RAG and 1IWL, respectively). D) SEC trace of $LolA^{WT}$ and $LolA^{P65T}$ with area under the curve calculations. E) SEC trace of dual proline GerS variants. Peaks are labeled with either “D” for dimer or “M” for monomer.

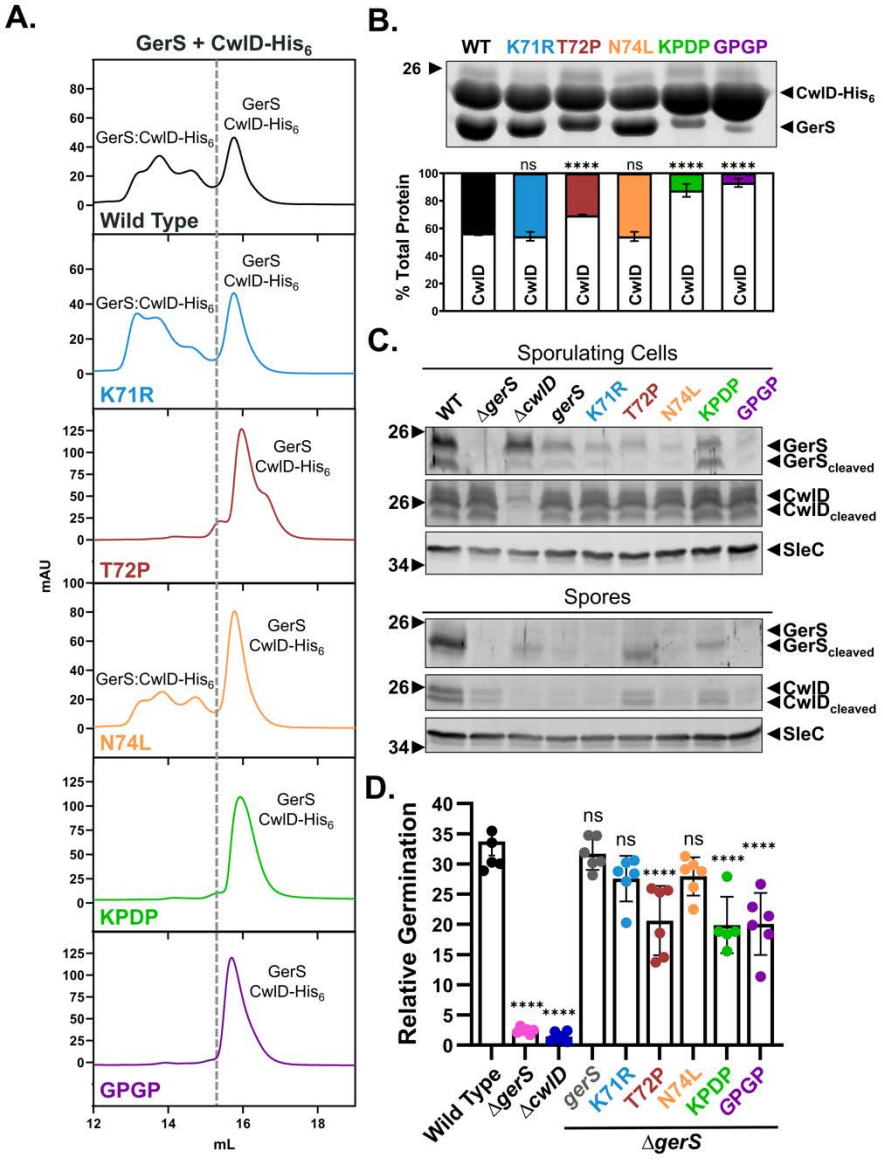

Figure 5. GerS substitutions that reduce dimerization decrease binding to CwlD and spore germination. A) SEC traces of GerS hinge region variants copurified with His_6-tagged CwlD. Peaks labeled with "GerS:CwlD-His_6", correspond to the complex formed between GerS and CwlD-His_6. Peaks labeled with "GerS" and "CwlD-His_6", represent the individual proteins that elute outside of complex. B) Coomassie stain of untagged GerS variants copurified with His_6-tagged CwlD. C) Western blot analyses of sporulating cell or purified spore lysates prepared from Δ*gerS* complemented with constructs encoding GerS hinge region variants. SleC was used as a loading control. D) Relative germination based on the change in optical density (OD_{600}) of purified spores over time following the addition of 1% (19 mM) taurocholate in rich media. Germination in arbitrary units was calculated using the area below inverted OD_{600} curves. Each *gerS* mutant is expressed by its native promoter in the *pyrE* locus in a Δ*gerS* background. A one-way ANOVA followed by Dunnett's multiple comparisons test was used to

842 compare the mean of each *gerS* mutant to the Δ*gerS*/*gerS* complement strain based on a
843 minimum of three biological replicates. Significance relative to WT is shown. (**** $p < 0.00005$).

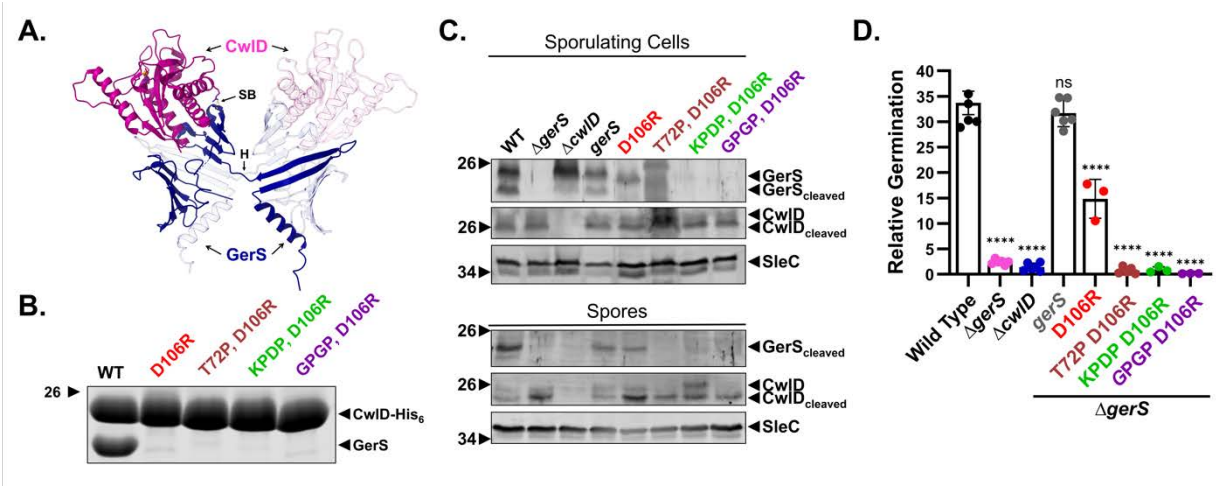

Figure 6. GerS interaction with CwlD is dependent on both strand-swapping and a salt bridge. A) GerS:CwlD structure (7RAG). SB, Salt bridge; H, Hinge. B) Coomassie-stained eluates of untagged homodimer-disrupting GerS variants combined with the salt bridge mutation D106R copurified with His_6-tagged CwlD. C) Relative germination calculated by area under the percent change in OD600 curve of spores in BHIS in the presence of 1% taurocholate over 1.5 hours. Each *gerS* mutant is expressed by its native promoter in the *pyrE* locus in a Δ*gerS* background. A one-way ANOVA followed by Dunnett's multiple comparisons test was used to compare each *gerS* mutant mean to the mean Δ*gerS*/*gerS* complement strain. Each mean is calculated from at least three biological replicates. Germination assay and statistics were run with Figure 5D, therefore Wild Type, Δ*gerS*, Δ*cwlD,* and Δ*gerS/gerS* complement are the same between both panels. The significance relative to WT is shown. (**** $p < 0.00005$). D) Detection of GerS variants by western blotting of sporulating cell or purified spore lysates. Polyclonal antibodies against GerS, CwlD, and SleC were used.